AIAA JOURNAL
Vol. 39, No. 11, November 2001

Time-Discontinuous Stabilized Space–Time Finite Elements for Timoshenko Beams

Boris A. Grohmann,* Thomas Wallmersperger,† and Bernd-Helmut Kröplin‡
University of Stuttgart, D-70569 Stuttgart, Germany
and
Rolf Dornberger§
ABB-ALSTOM Technology, Ltd., CH-5405 Baden-Dättwil, Switzerland

Stabilized space–time finite element methods for the transient computational analysis of the elastodynamics of Timoshenko beams have been developed. The underlying time-discontinuous Galerkin formulation is implicit, unconditionally stable, higher-order accurate, and robust. The employed interpolations are continuous in space and time inside time slabs, but discontinuous in time between adjacent time slabs. To suppress spurious numerical oscillations near discontinuities or high gradients, Galerkin/least-squares stabilization has been applied. Further improvement of the numerical representation of the transient elastic wave propagation phenomena has been achieved by specially designed Galerkin/gradient least-squares operators. Because of the reduced phase and amplitude errors of these finite elements, much coarser spatial meshes may be used without loss of accuracy. The resulting reduction of the number of unknowns leads to a significant decrease of computer time. Furthermore, a global adaptive time-stepping strategy has been employed based on the temporal jump residual of the time finite element method as error estimator. Numerical examples of transient elastic wave propagation in Timoshenko beams involving a wide spectrum of wave numbers and frequencies demonstrate the good performance of the developed methods.

Nomenclature

A	=	cross section area
A_s	=	κA, where $\kappa = \frac{5}{6}$
$\boldsymbol{A}$	=	amplification matrix
b	=	damping
C	=	Courant number
$\boldsymbol{C}$	=	damping matrix
c	=	wave speed
E	=	elastic modulus
$\boldsymbol{f}$	=	load vector
G	=	shear modulus
I	=	moment of inertia
I_N	=	time interval
$\boldsymbol{K}$	=	stiffness matrix
$\mathcal{L}$	=	differential operator
m	=	moment load
M	=	bending moment
$\boldsymbol{M}$	=	mass matrix
N	=	normal force
p	=	pressure load
Q	=	transverse force
Q_N	=	Nth space–time slab
T	=	period of oscillation
t	=	time coordinate
t_n	=	time level
$\boldsymbol{U}$	=	vector of unknowns
u	=	longitudinal displacement
$\boldsymbol{u}$	=	vector of displacement unknowns
$\boldsymbol{v}$	=	vector of velocity unknowns
$\boldsymbol{W}$	=	vector of weightings
w	=	vertical (bending) displacement
$\boldsymbol{w}_1, \boldsymbol{w}_2$	=	vector of displacement and velocity weightings
x	=	space coordinate
$\Gamma(t)$	=	spatial boundary
γ	=	shear strain
Δt	=	time step
Δx	=	spatial element length
δ	=	variation
ϵ	=	longitudinal strain
κ	=	curvature
λ_i	=	complex eigenvalue of the amplification matrix $\boldsymbol{A}$
ρ	=	density
ρ	=	spectral radius
$\boldsymbol{\tau}$	=	matrix of intrinsic time scales
$\boldsymbol{\Phi}$	=	space–time interpolation
φ	=	slope
$\Omega(t)$	=	spatial domain
ω	=	$2\pi/T$ frequency

Subscripts and Superscripts

$a\|_n^{\pm}$	=	$\lim_{\varepsilon \to 0} a(t_n \pm \varepsilon)$, where $\varepsilon > 0$
T	=	transposition of vector or matrix
x, y, z	=	directions in space
$\hat{}$	=	nodal value
$*$	=	modified value

Received 8 November 1999; revision received 1 April 2001; accepted for publication 2 April 2001.

*Ph.D. Student, Institut für Statik und Dynamik der Luft- und Raumfahrtkonstruktionen, Pfaffenwaldring 27; boris@xi-grohmann.de. Member AIAA.
†Ph.D. Student, Institut für Statik und Dynamik der Luft- und Raumfahrtkonstruktionen, Pfaffenwaldring 27; wallmers@isd.uni-stuttgart.de.
‡Professor, Head of Institut für Statik und Dynamik der Luft- und Raumfahrtkonstruktionen, Pfaffenwaldring 27.
§Scientist, Abteilung Thermo und Aerodynamik, Segelhof.

I. Introduction

THE finite element method (FEM) has been used for structural mechanics for many years. Nevertheless, for transient computations semidiscrete methods using FEM in space and finite difference methods in time, such as the Newmark algorithm, are most commonly applied.

Lesaint and Raviart[1] have introduced space–time finite elements based on the time-discontinuous Galerkin (TDG) approach for solving the neutron transport equation. The method yields implicit, unconditionally stable, and higher-order accurate discretization. Hughes and Hulbert[2] have applied the TDG method for elastodynamics. Johnson[3] and Hulbert[4] have investigated the TDG formulation for second-order hyperbolic problems in time.

Hughes and Hulbert[2] also have applied Galerkin/least-squares (GLS) stabilization terms in order to improve the stability of the underlying TDG for elastodynamics. Franca and Dutra Do Carmo[5] have introduced the Galerkin/gradient least-squares (G∇LS) method for scalar singular diffusion problems to improve the accuracy. Grosh and Pinsky[6] have designed the spatial G∇LS operator for time-harmonic oscillations of Timoshenko beams to meet specific design criteria such as minimal dispersion error. Li and Wiberg[7] have developed global time-stepping algorithms for structural dynamics. Thompson and Pinsky[8] and Thompson[9] have given a space–time finite element formulation for structural acoustics. Grohmann et al.[10] and Grohmann and Dinkler[11] have applied the stabilized space–time finite element approach to coupled fluid–structure simulations in the field of aeroelasticity.

The aim of the present research is the development of a time-accurate space–time FEM for Timoshenko beams with additional stabilization to improve the accuracy of the transient elastic wave propagation. Space–time adaptivity has been applied to increase the efficiency of the numerical method.

In Sec. II the underlying nonlinear Timoshenko beam model is described. The space–time finite element formulation is introduced in Sec. III. When the GLS stabilization of Sec. IV is generalized, the optimized G∇LS design is derived in Sec. V. Various strategies for adaptivity in space and time are discussed in Sec. VII. Finally, some results are given in Sec. VIII.

II. Nonlinear Structural Dynamics

The mathematical analysis of the dynamics of elastic structures leads to equations of motion that may be devised in the following matrix form:

$$\boldsymbol{M}\ddot{\boldsymbol{u}} + \boldsymbol{C}\dot{\boldsymbol{u}} + \boldsymbol{K}(\boldsymbol{u})\boldsymbol{u} - \boldsymbol{f} = \boldsymbol{0} \tag{1}$$

where $\boldsymbol{u}$ are the structural displacement unknowns. The symmetric mass matrix $\boldsymbol{M}$ may be assumed to be positive definite, but the nonlinear stiffness operator $\boldsymbol{K}(\boldsymbol{u})$ may lead to indefinite stiffness matrices.

To investigate structural dynamics including wave propagation, the Timoshenko beam model is considered. The principle of virtual power yields the following weak form:

$$\int_{I_N}\int_{\Omega(t)} \delta\dot{\epsilon}N + \delta\dot{u}\{\rho A\ddot{u} + bA\dot{u} - p_x\} + \delta\dot{\gamma}Q + \delta\dot{w}\{\rho A\ddot{w} + bA\dot{w} - p_z\} + \delta\dot{\kappa}M + \delta\dot{\varphi}\{\rho I\ddot{\varphi} + bI\dot{\varphi} - m\}\,\mathrm{d}\Omega\,\mathrm{d}t = 0 \tag{2}$$

where the geometrically nonlinear strains

$$\epsilon = u_{,x} + \tfrac{1}{2}w_{,x}^2, \qquad \gamma = w_{,x} + \varphi, \qquad \kappa = \varphi_{,x} \tag{3}$$

and the forces and moments

$$N = EA\epsilon, \qquad Q = GA_s\gamma, \qquad M = EI\kappa \tag{4}$$

are employed.

The integration is carried out over the time interval $I_N = \{t\,|\,t_n \le t \le t_{n+1}\}$ and the entire spatial domain $\Omega(t) = \{x\,|\,x_{\min}(t) \le x \le x_{\max}(t)\}$ of the beam (Fig. 1). Appropriate natural (traction) boundary conditions and essential (displacement) boundary conditions are applied on $\Gamma = \partial\Omega$.

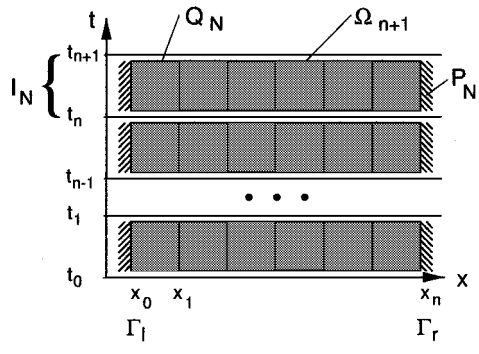

Fig. 1 Space–time domain.

Furthermore, an initial shape u_0, w_0, and φ_0 is considered according to

$$u = u_0 + u', \qquad w = w_0 + w', \qquad \varphi = \varphi_0 + \varphi' \tag{5}$$

where u', w', and φ' represent the relative displacements and u, w, and φ give the resulting total shape. In the case of $u' = w' = \varphi' = 0$, the structure is assumed to be stress free.

The linear Timoshenko beam model allows wave propagation with two different wave speeds,

$$c_1 = \sqrt{E/\rho}, \qquad c_2 = \sqrt{G/\rho} \tag{6}$$

III. Space–Time Finite Element Formulation

Space–time interpolations $\Phi_j(\boldsymbol{x}, t)$ are used for both the weights $\boldsymbol{W}_h$ and the unknowns $\boldsymbol{U}_h$:

$$\boldsymbol{W}_h(\boldsymbol{x}, t) = \sum_{j=1}^{M} \Phi_j(\boldsymbol{x}, t)\hat{\boldsymbol{W}}_j \tag{7a}$$

$$\boldsymbol{U}_h(\boldsymbol{x}, t) = \sum_{j=1}^{M} \Phi_j(\boldsymbol{x}, t)\hat{\boldsymbol{U}}_j \tag{7b}$$

where $\hat{\boldsymbol{W}}_j$ and $\hat{\boldsymbol{U}}_j$ are the nodal values.

Note that the interpolations for the TDG formulation are continuous in space, but discontinuous in time between adjacent time slabs.

A. Single-Field Formulation

The TDG formulation for elastodynamics is based on the principle of virtual power Eq. (2):

$$\int_{I_n} \dot{\boldsymbol{w}}^T \cdot \{\boldsymbol{M}\ddot{\boldsymbol{u}} + \boldsymbol{C}\dot{\boldsymbol{u}} + \boldsymbol{K}\boldsymbol{u} - \boldsymbol{f}\}\,\mathrm{d}t + \boldsymbol{w}^T|_n^+\left\{\boldsymbol{K}\boldsymbol{u}|_n^+ - \boldsymbol{K}\boldsymbol{u}|_n^-\right\} + \dot{\boldsymbol{w}}^T|_n^+\left\{\boldsymbol{M}\dot{\boldsymbol{u}}|_n^+ - \boldsymbol{M}\dot{\boldsymbol{u}}|_n^-\right\} = \boldsymbol{0} \tag{8}$$

The integral represents the energy conservation inside the time slab, whereas the second and third terms, referred to as temporal jump term or temporal jump residual (TJR), enforce the continuity of the potential and kinetic energy between subsequent time slabs in a weak sense. For these terms, the notation $a|_n^{\pm} = \lim_{\varepsilon \to 0} a(t_n \pm \varepsilon)$ has been introduced.

Note that system (8) cannot be solved for singular stiffness matrices $\boldsymbol{K}$.

B. Two-Field Formulation

In the case of the two-field formulation, the differential equation of second order in time [Eq. (1)] is transformed to a system of first order in time. The equation of motion is written as

$$\boldsymbol{M}\dot{\boldsymbol{v}} + \boldsymbol{C}\boldsymbol{v} + \boldsymbol{K}\boldsymbol{u} - \boldsymbol{f} = \boldsymbol{0} \tag{9}$$

A second operator enforces the identity

$$\dot{\boldsymbol{u}} - \boldsymbol{v} = \boldsymbol{0} \tag{10}$$

in weak form. To introduce the TDG method, independent interpolations for the structural displacement $\boldsymbol{u}$ and velocity unknowns $\boldsymbol{v}$ and the respective weighting functions $\boldsymbol{w}_1$ and $\boldsymbol{w}_2$ are employed. This yields

$$\int_{I_N} \left[\boldsymbol{w}_1^T, \boldsymbol{w}_2^T\right] \cdot \left\{ \begin{bmatrix} \boldsymbol{K} & \boldsymbol{0} \\ \boldsymbol{0} & \boldsymbol{M} \end{bmatrix} \begin{bmatrix} \dot{\boldsymbol{u}} \\ \dot{\boldsymbol{v}} \end{bmatrix} + \begin{bmatrix} \boldsymbol{0} & -\boldsymbol{K} \\ \boldsymbol{K} & \boldsymbol{C} \end{bmatrix} \begin{bmatrix} \boldsymbol{u} \\ \boldsymbol{v} \end{bmatrix} - \begin{bmatrix} \boldsymbol{0} \\ \boldsymbol{f} \end{bmatrix} \right\} \mathrm{d}t + \left[\boldsymbol{w}_1^T, \boldsymbol{w}_2^T\right]\Big|_n^+ \left\{ \begin{bmatrix} \boldsymbol{K}\boldsymbol{u} \\ \boldsymbol{M}\boldsymbol{v} \end{bmatrix}_n^+ - \begin{bmatrix} \boldsymbol{K}\boldsymbol{u} \\ \boldsymbol{M}\boldsymbol{v} \end{bmatrix}_n^- \right\} = \boldsymbol{0} \tag{11}$$

The second hyperrow of the domain integral represents the equation of motion (9), whereas the first hyperrow corresponds to Eq. (10).

Table 1 Comparison of TDG method with different interpolations

Method	Interpolation of $\boldsymbol{u}$	Amplitude error of $\boldsymbol{u}$	Unknowns
$P2$	Quadratic	$\sim \Delta t^3$	3
$P1$–$P1$	Linear	$\sim \Delta t^3$	4
$P3$	Cubic	$\sim \Delta t^5$	4
$P2$–$P2$	Quadratic	$\sim \Delta t^5$	6

Similar to the single-field formulation, the last term, the TJR, enforces the continuity of kinetic and potential energy between subsequent time slabs.

Equation (11) shows that the system of equations becomes singular when rigid-body motions occur or in the case of buckling. This can be avoided by an appropriate preconditioning of the weighting functions or, in case of linear physics, by static condensation.

C. Comparison

Table 1 shows a comparison of the TDG space–time finite element formulation for structural dynamics. Pi denotes the single-field formulation employing ith-order polynomials $\mathcal{P}^i$ in time for the displacements $\boldsymbol{u}$. Pi–Pj represents the two-field formulation employing $\mathcal{P}^i$ for the displacements $\boldsymbol{u}$ and $\mathcal{P}^j$ for the velocities $\boldsymbol{v}$.

In the case of linear physics, the number of unknowns of the formulations may be reduced by static condensation.[4,7]

In the special case of the two-field formulation when the interpolations for the displacements are taken one order higher than for the velocities, the equivalence $\dot{\boldsymbol{u}} = \boldsymbol{v}$ may be satisfied exactly, and a new equivalent single-field formulation for elastodynamics is obtained.[12] While maintaining the accuracy and stability of the scheme [Eq. (8)] the number of unknowns of the new method is reduced for both linear and nonlinear problems.

IV. GLS Stabilization

The standard (Bubnov–) Galerkin method just presented is based on the residual of the underlying partial differential equation. In the case of the GLS method, an additional term based on the square of the residual is added to stabilize the numerical scheme. By this means, high-frequency/short-wavelength spurious oscillations are suppressed while the accuracy and order of convergence of the underlying standard Galerkin method are preserved.[2]

A. Two-Field Formulation

In the case of the two-field formulation, the differential operators

$$\mathcal{L}_1 \boldsymbol{U} := \boldsymbol{M}\dot{\boldsymbol{v}} + \boldsymbol{C}\boldsymbol{v} + \bar{\boldsymbol{K}}\boldsymbol{u} \tag{12a}$$

$$\mathcal{L}_2 \boldsymbol{U} := \dot{\boldsymbol{u}} - \boldsymbol{v} \tag{12b}$$

are introduced. The time-discontinuous GLS method is given as

$$\int_{I_N} \boldsymbol{w}_2^T \{\boldsymbol{M}\dot{\boldsymbol{v}} + \boldsymbol{C}\boldsymbol{v} + \boldsymbol{K}\boldsymbol{u} - \boldsymbol{f}\} + \boldsymbol{w}_1^T \boldsymbol{K}\mathcal{L}_2\boldsymbol{U} + \{\boldsymbol{\tau}_1\mathcal{L}_1\boldsymbol{W}\}^T\{\mathcal{L}_1\boldsymbol{U} - \boldsymbol{f}\}$$
$$+ \{\boldsymbol{\tau}_2\mathcal{L}_2\boldsymbol{W}\}^T \boldsymbol{K}\mathcal{L}_2\boldsymbol{U}\,\mathrm{d}t + \boldsymbol{w}_1^T|_n^+ \left\{\boldsymbol{K}\boldsymbol{u}|_n^+ - \boldsymbol{K}\boldsymbol{u}|_n^-\right\}$$
$$+ \boldsymbol{w}_2^T|_n^+ \left\{\boldsymbol{M}\boldsymbol{v}|_n^+ - \boldsymbol{M}\boldsymbol{v}|_n^-\right\} = \boldsymbol{0} \tag{13}$$

where the boundary terms resulting from integration by parts of the stiffness matrix $\boldsymbol{K}$ of the standard Galerkin term have been dropped for conciseness.

To build the least-squares operator of the equation of motion, it is necessary to employ the nonsymmetric stiffness operator $\bar{\boldsymbol{K}}$ instead of the symmetric $\boldsymbol{K}$. $\bar{\boldsymbol{K}}$ is based on the partial differential equation before integration by parts.

Note that the GLS stabilization of the equation of motion (12a) leads to additional terms in both hyperrows, that is, affects the weak form of both the equation of motion itself and the identity Eq. (10). The least squares of Eq. (12b) also modifies both rows.

The matrices of intrinsic timescales for the general, nonlinear case

$$\boldsymbol{\tau}_1 = \frac{\partial \tau}{\partial t}\left\{\left\|\left(\frac{\partial \tau}{\partial t}\right)^2 \boldsymbol{M}\right\|^m + \left\|\frac{\partial \tau}{\partial t}\boldsymbol{C}\right\|^m + \|\boldsymbol{K}\|^m\right\}^{-1/m} \tag{14a}$$

$$\boldsymbol{\tau}_2 = \left\{\frac{\partial \tau}{\partial t}\right\}^{-1} \boldsymbol{I} \tag{14b}$$

are obtained from analyzing the magnitudes of all contributing terms. The generalized norm $\|\ \|^m$, where $m \in \{1, 2, \infty\}$, has been introduced according to Soulaimani and Fortin.[13] Note the leading factor $\partial\tau/\partial t$ in Eq. (14a), which stems from the principle of virtual power. Equation (14a) is a generalization to structural dynamics of the definition for τ developed in the framework of compressible flows by Shakib.[14]

In the case of the linear Timoshenko beam with the unknowns $\boldsymbol{u} = [w, \varphi]$, the matrices

$$\boldsymbol{M} = \begin{bmatrix} \rho A & 0 \\ 0 & \rho I \end{bmatrix} \tag{15a}$$

$$\boldsymbol{C} = \begin{bmatrix} bA & 0 \\ 0 & bI \end{bmatrix} \tag{15b}$$

$$\boldsymbol{K} = \begin{bmatrix} {}_x\partial GA_s\partial_x & {}_x\partial GA_s \\ GA_s\partial_x & {}_x\partial EI\partial_x + GA_s \end{bmatrix} \tag{15c}$$

$$\bar{\boldsymbol{K}} = \begin{bmatrix} -GA_s\partial_{xx} & -GA_s\partial_x \\ GA_s\partial_x & -EI\partial_{xx} + GA_s \end{bmatrix} \tag{15d}$$

are obtained. Because of the second-order spatial derivatives in $\bar{\boldsymbol{K}}$, at least quadratic interpolations in space are necessary. When Eqs. (14) are applied to the linear case, the matrices of intrinsic timescales

$$\boldsymbol{\tau}_1 = \begin{bmatrix} \tau_{1w} & 0 \\ 0 & \tau_{1\varphi} \end{bmatrix} \tag{16a}$$

$$\boldsymbol{\tau}_2 = \begin{bmatrix} \tau_2 & 0 \\ 0 & \tau_2 \end{bmatrix} \tag{16b}$$

where

$$\tau_{1w} = \frac{2}{\Delta t}\left\{\left\|\frac{4\rho A}{\Delta t^2}\right\|^m + \left\|\frac{2bA}{\Delta t}\right\|^m + 2\left\|\frac{4GA_s}{\Delta x^2}\right\|^m\right\}^{-1/m}$$

$$\tau_{1\varphi} = \frac{2}{\Delta t}\left\{\left\|\frac{4\rho I}{\Delta t^2}\right\|^m + \left\|\frac{2bI}{\Delta t}\right\|^m + \left\|\frac{4EI}{\Delta x^2}\right\|^m + 2\|GA_s\|^m\right\}^{-1/m}$$

$$\tau_2 = \frac{1}{2}\Delta t$$

are employed for the numerical examples of Sec. VIII. Similar formulas may be derived following Hulbert[15] using the wave speeds according to Eq. (6).

B. Single-Field Formulation

The stabilized single-field formulation

$$\int_{I_N} \dot{\boldsymbol{w}}^T\{\boldsymbol{M}\ddot{\boldsymbol{u}} + \boldsymbol{C}\dot{\boldsymbol{u}} + \boldsymbol{K}\boldsymbol{u} - \boldsymbol{f}\} + \{\boldsymbol{\tau}_1\mathcal{L}\boldsymbol{w}\}^T\{\mathcal{L}\boldsymbol{u} - \boldsymbol{f}\}\,\mathrm{d}t$$
$$+ \boldsymbol{w}^T|_n^+ \left\{\boldsymbol{K}\boldsymbol{u}|_n^+ - \boldsymbol{K}\boldsymbol{u}|_n^-\right\} + \dot{\boldsymbol{w}}^T|_n^+ \left\{\boldsymbol{M}\dot{\boldsymbol{u}}|_n^+ - \boldsymbol{M}\dot{\boldsymbol{u}}|_n^-\right\} = \boldsymbol{0}$$

where

$$\mathcal{L}\boldsymbol{u} := \boldsymbol{M}\ddot{\boldsymbol{u}} + \boldsymbol{C}\dot{\boldsymbol{u}} + \bar{\boldsymbol{K}}\boldsymbol{u} \tag{17}$$

may be obtained from Eq. (13) by choosing the interpolations for the displacements $\boldsymbol{u}$ and $\boldsymbol{w}_1$ one order higher in time than the interpolations for the velocities $\boldsymbol{v}$ and $\boldsymbol{w}_2$ and by explicitely setting $\mathcal{L}_2\boldsymbol{U} = \boldsymbol{0}$.

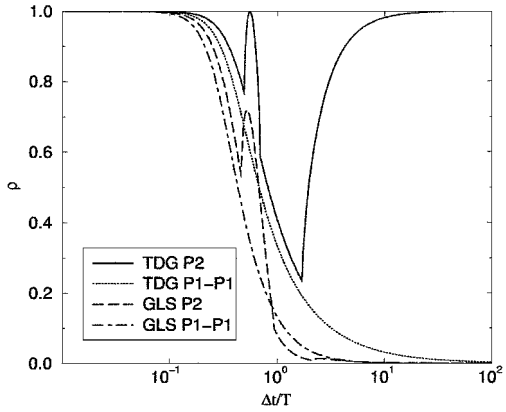

Fig. 2 Filtering characteristics.

C. Comparison

Figure 2 shows the temporal filtering characteristics of several single-field and two-field schemes for a physically undamped single-degree-of-freedom (DOF) oscillator of scalar mass m and stiffness k with the period of oscillation $T = 2\pi\sqrt{(m/k)}$. The matrices of intrinsic timescales for the GLS formulations have been chosen as $\tau_1 = \Delta t/2m$ and $\tau_2 = \Delta t/2$.

Expressing the discrete unknowns $\boldsymbol{u}|_{n+1}^-$ and $\boldsymbol{v}|_{n+1}^-$ at the end of time slab I_N in terms of the corresponding initial conditions $\boldsymbol{u}|_n^-$ and $\boldsymbol{v}|_n^-$ yields

$$\begin{bmatrix} \boldsymbol{u}|_{n+1}^- \\ \Delta t\boldsymbol{v}|_{n+1}^- \end{bmatrix} = \boldsymbol{A} \begin{bmatrix} \boldsymbol{u}|_n^- \\ \Delta t\boldsymbol{v}|_n^- \end{bmatrix} \tag{18}$$

where $\boldsymbol{A}$ is the amplification matrix. The spectral radius ρ of $\boldsymbol{A}$ is defined as

$$\rho(\boldsymbol{A}) = \max_i(|\lambda_i(\boldsymbol{A})|) \tag{19}$$

where λ_i are the eigenvalues of $\boldsymbol{A}$. The spectral radius is a measure for the artificial, numerical damping.

Because all schemes are unconditionally stable, the numerically computed amplitude is always less than or equal the exact amplitude, that is, $\rho \le 1$. For sufficient resolution, $\Delta t/T \ll 1$, the amplitude error approaches zero and $\rho \to 1$. For resolutions with less than 10 time steps per period ($\Delta t/T > 0.1$), the numerical damping becomes significant. For less than approximately four time steps per period the physical oscillations are not adequately resolved. For $\Delta t/T \gg 1$, the two-field and single-field formulations show completely different damping characteristics: whereas the two-field TDG methods annihilate the underresolved scales [$\lim_{\Delta t/T\to\infty} \rho(\Delta t/T) = 0$], the single-field TDG methods preserve their amplitudes, that is, $\lim_{\Delta t/T\to\infty} \rho(\Delta t/T) = 1$ (see also Hulbert[4,16]).

It is well known that underresolved scales may spoil the overall solution if they are not dampened.[17] For this reason, the high-frequency filtering characteristics of the two-field formulations are desirable. To obtain asymptotic annihilation for both single- and two-field TDG methods, GLS stabilization may be applied (see Sec. IV).

A comparison of several TDG methods and the Newmark scheme may be found by Li and Wilberg[7] and Wallmersperger.[18]

V. Galerkin/Generalized Least Squares

The formulation according to Sec. IV with the given choice of $\boldsymbol{\tau}_1$ and $\boldsymbol{\tau}_2$ serves to increase stability and robustness and to reduce spurious oscillations without loss of accuracy.

Further generalizations of this idea are possible. In the G∇LS method by Franca and Dutra Do Carmo[5] the square of the gradient of the residual is minimized by adding an operator of the form

$$\int_{Q_N} \{\boldsymbol{\tau}\nabla\mathcal{L}\boldsymbol{W}\}^T\{\nabla(\mathcal{L}\boldsymbol{U} - \boldsymbol{f})\}\,\mathrm{d}Q \tag{20}$$

Note the consistency of the resulting method because the additional term is proportional to the residual. The minimization of the gradient may be interpreted as an attempt to achieve equal distribution of the residual in the whole field.

It is possible to design stabilization operators to achieve certain optimal characteristics of the resulting numerical scheme, for example, minimal phase or amplitude errors. The starting point for the present analysis is the G∇LS formulation by Grosh and Pinsky.[6] They investigate time-harmonic oscillations of undamped linear Timoshenko beams in the frequency domain

$$(\boldsymbol{K} - \omega^2\boldsymbol{M})\boldsymbol{u} = \boldsymbol{f} \tag{21}$$

Their G∇LS formulation leads to the following modified equation:

$$(\boldsymbol{K} - \omega^2\boldsymbol{M} + \tilde{\boldsymbol{K}})\boldsymbol{u} = \boldsymbol{f} + \tilde{\boldsymbol{f}} \tag{22}$$

In the present contribution, their approach is extended to the simulation of nonharmonic oscillations in the time domain. For linear interpolations in space combined with the third-order TDG time-stepping schemes, the resulting discretization for the present transient wave propagation problem exhibits severe dispersion error. The space–time error analysis shows that this error stems from the low-order spatial discretization.

Applying the G∇LS in space, the modified equation of the form

$$(\boldsymbol{K} + \boldsymbol{K}^*)\boldsymbol{u} + (\boldsymbol{M} + \boldsymbol{M}^*)\ddot{\boldsymbol{u}} = \boldsymbol{f} + \boldsymbol{f}^* \tag{23}$$

similar to Eq. (22) is obtained, where

$$\boldsymbol{K}^* = \begin{bmatrix} s_1 & 0 & -s_1 & 0 \\ 0 & s_2 & 0 & -s_2 \\ -s_1 & 0 & s_1 & 0 \\ 0 & -s_2 & 0 & s_2 \end{bmatrix} \tag{24a}$$

$$\boldsymbol{M}^* = \begin{bmatrix} t_1 & 0 & -t_1 & 0 \\ 0 & t_2 & 0 & -t_2 \\ -t_1 & 0 & t_1 & 0 \\ 0 & -t_2 & 0 & t_2 \end{bmatrix} \tag{24b}$$

To apply the TDG time-stepping schemes [Eqs. (8) and (11)] to the modified equation Eq. (23), $\boldsymbol{M}$ and $\boldsymbol{K}$ have to be substituted for by $\boldsymbol{M} + \boldsymbol{M}^*$ and $\boldsymbol{K} + \boldsymbol{K}^*$, respectively. Note that this also leads to a modification of the temporal jump operators.

Doing a Fourier analysis of the spatial discretization, applying a Taylor series expansion, and annihilating the lowest-order error terms in the resulting Fourier matrix gives

$$s_1 = 0, \qquad s_2 = \tfrac{1}{6}GA_s\Delta x, \qquad t_1 = \tfrac{1}{6}\rho A\Delta x, \qquad t_2 = \tfrac{1}{6}\rho I\Delta x \tag{25}$$

Unfortunately, the present choice (G∇LS$_L$) of s_2 leads to locking. If we keep the mass matrix stabilization terms and apply selective reduced integration of the stiffness matrix, we get the coefficients for enhanced Fourier matrix accuracy (G∇LS$_\mathcal{F}$) similar to Grosh and Pinsky[6]:

$$s_1 = 0, \qquad s_2 = -\tfrac{1}{12}GA_s\Delta x$$

$$t_1 = \tfrac{1}{6}\rho A\Delta x, \qquad t_2 = \tfrac{1}{6}\rho I\Delta x \tag{26}$$

As an alternative, the zero dispersion error operator by Grosh and Pinsky,[6] which depends on ω, may be applied. For unsteady problems including a large spectrum of frequencies, the dependency of the stabilization on ω has to be eliminated. Optimizing the representation of low-frequency waves, we transfer their operator for $\omega \to 0$ (G∇LS$_{\omega\to 0}$) and get

$$s_1 = 0, \qquad s_2 = -\frac{1}{12}GA_s\Delta x, \qquad t_1 = \frac{1}{4}\rho A\Delta x$$

$$t_2 = -\rho\Delta x\left(\frac{-EAI}{6GA_s} + \frac{I}{12} + \frac{7A\Delta x^2}{360}\right) \tag{27}$$

The present spatial G∇LS operator applied to the equation of motion leads to a significant improvement of the spatial resolution. This stems from the correction of the dispersion error resulting from the spatial discretization. The phase error of the TDG itself is much smaller, and so the time-stepping scheme has not been modified.

Note that the $\boldsymbol{K}^*$ in both cases is equivalent to the $\tilde{\boldsymbol{K}}$ obtained by Grosh and Pinsky[6] for selective reduced integration.

VI. Discontinuity Capturing

The least-squares and generalized least-squares operators introduced earlier increase stability and accuracy. Nevertheless, they do not guarantee monotonic solutions near spatial or temporal discontinuities. For this purpose, a nonlinear, consistent artificial viscosity operator of the generic form

$$\int_{Q_N} \{\nabla \boldsymbol{W}\}^T \boldsymbol{\nu} \nabla \boldsymbol{U}\, \mathrm{d}\boldsymbol{Q} \tag{28}$$

may be introduced. The discontinuity capturing (DC) artificial viscosity is proportional to powers of the residual $\|\boldsymbol{\nu}(\boldsymbol{U})\| \sim \|\mathcal{L}\boldsymbol{U} - \boldsymbol{f}\|^m$. Thus, the consistency of the operator is guaranteed, and the artificial viscosity quickly decreases in areas where the solution is smooth.[14]

The nonlinear DC viscosity may be chosen according to Hulbert[15]

$$\boldsymbol{\nu}(\boldsymbol{U}) \sim \frac{\|\mathcal{L}\boldsymbol{U} - \boldsymbol{f}\|^m}{\|\nabla \boldsymbol{U}\|^m} \tag{29}$$

or similar to the formulation of Barth and Sethian[19]

$$\boldsymbol{\nu}(\boldsymbol{U}) \sim \frac{\|\mathcal{L}\boldsymbol{U} - \boldsymbol{f}\|}{\{\|\boldsymbol{M}\ddot{\boldsymbol{u}}\|^m + \|\boldsymbol{C}\dot{\boldsymbol{u}}\|^m + \|\boldsymbol{K}\boldsymbol{u}\|^m + \|\boldsymbol{f}\|^m\}^{1/m}} \tag{30}$$

Shock-capturing operators similar to the preceding formulations were originally developed in the context of compressible fluid mechanics to improve the resolution of compression shocks and contact discontinuities. There, the underlying physics of the problem are quite different from linear elastodynamics: Compressible flows have the property of self-sharpening, that is, an initially small and smooth wave may become a discontinuity as a result of nonlinear convection.

Hulbert[15] has developed DC operators in the context of the single-field formulation for elastodynamics. The present investigations with Timoshenko beams indicate that for high Courant numbers,

$$C_i = c_i \Delta t / \Delta x > 1 \tag{31}$$

the asymptotic annihilation of high-frequency oscillations by the two-field formulation helps to resolve adequately sharp gradients of the solution with only few spurious oscillations. Nevertheless, for low Courant numbers, $C_i \approx 1$, the additional DC operator is advisable. However, in the context of linear physics, nonlinear DC operators significantly increase cost due to the necessity of nonlinear iteration.

VII. Space–Time Adaptivity

Most real world problems involve different spatial or temporal scales. Concerning structural dynamics and elastodynamics, large-scale modes concern the global deformations of a structure with low frequency. The fine-scale modes represent high-frequency and short-wavelength elastic wave propagation phenomena.

For engineering analysis, relevant large scales and irrelevant small scales have to be distinguished. Classically, this results in the engineering decision on the required spatial and temporal mesh resolution. Problems arise if the character of the solution is not known a priori or in the case if local fine-scale phenomena are crucial for the large-scale solution. In the first case, an automatic, solution-dependent refinement of the space–time mesh is desirable, whereas locally restricted refinement is necessary in the latter situation.

Different strategies of adaptive refinement have to be distinguished. The spatial or temporal size of the finite elements (h adaptivity) or the order of the finite element interpolations (p adaptivity) may be adapted to the character of the solution.

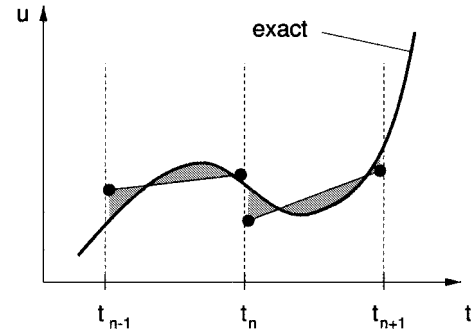

Fig. 3 Interpolation error and temporal jump at the interface between time slabs.

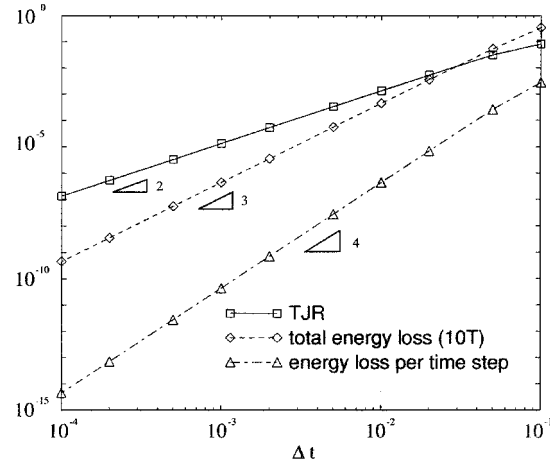

Fig. 4 Order of convergence of TJR, local and global loss of energy for a single-DOF spring–mass oscillator using the $P1$–$P1$ method.

Self-adaptive refinement requires an error estimator, that is, the numerical method requires a mathematical statement concerning local or global accuracy. Different error indicators such as the local gradient of the solution, for example, for DC in compressible fluid mechanics, or the finite element local residual may be used.

In the context of TDG space–time finite elements, the residual of the weakly enforced initial conditions may be employed as error indicator. This TJR is an estimator for the interpolation error inside the time slab (see Fig. 3). For time slab I_N, it can be computed a posteriori from the total jump of potential and kinetic energy:

$$\mathrm{TJR}_n = \tfrac{1}{2}\boldsymbol{u}^T\boldsymbol{K}\boldsymbol{u}|_n^+ - \tfrac{1}{2}\boldsymbol{u}^T\boldsymbol{K}\boldsymbol{u}|_n^- + \tfrac{1}{2}\boldsymbol{v}^T\boldsymbol{M}\boldsymbol{v}|_n^+ - \tfrac{1}{2}\boldsymbol{v}^T\boldsymbol{M}\boldsymbol{v}|_n^- \tag{32}$$

Because the TDG method is based on the principle of virtual power, conservation of momentum is a fundamental part of the formulation. On the contrary, the TJR guarantees unconditional stability in terms of decreasing total energy. For this reason, the TJR has been used as error indicator for time step control by Li and Wiberg[7] and Ruge.[20]

Figure 4 shows the convergence of the temporal jump residual and the corresponding energy loss for a single-DOF spring-mass oscillator using the $P1$–$P1$ method. In agreement with the overall order of convergence of the displacement and velocity unknowns, the computed total energy loss after 10 periods of oscillation is $\Delta e_{10T} \sim \Delta t^3$. Accordingly, the energy loss per time step is $\Delta e_{\Delta t} \sim \Delta t^4$. TJR $\sim \Delta t^2$, which is the same as the accuracy of the corresponding standard Galerkin method. The second-order error term of the standard Galerkin cancels out with the TJR when the initial conditions are enforced weakly, and thus, the TDG method is third-order accurate.

Concerning adaptivity, several variants are possible. The mesh may be adapted globally or locally. The combination of spatial and temporal adaptivity with the underlying finite element discretization is decisive for the accuracy of the resulting method.

A. Adaptive Global Time-Stepping Strategy

For the adaptive global time-stepping method, the spatial mesh is fixed. The global time step is adapted to the unsteady development of the solution to match the prescribed temporal accuracy requirements. One might desire to adapt the time step to resolve high-frequency phenomena or to resolve high gradients of the solution in time. For instance, the application of a short impulse load requires small time steps, whereas large time steps are desirable to reduce the computational effort for the long-term response (see Sec. VIII).

In the present research, the $\widetilde{\text{TJR}}$ is prescribed as an accuracy requirement. The time step for the next time slab I_{N+1} is estimated according to

$$\Delta t_{N+1} = \Delta t_N (\text{TJR}_n / \widetilde{\text{TJR}})^{1/m} \tag{33}$$

where Δt_N is the time step that has successfully been applied in the present time slab I_N meeting the accuracy requirement $\widetilde{\text{TJR}}$. The actual TJR_n may be computed in different norms, like the local maximum or the integral norm throughout the domain. The exponent m is chosen corresponding to the applied TDG method. According to Fig. 4, the theoretically correct value for the $P1$–$P1$ method is $m = 2$, but $m = 3$ works also.

There are several different possibilities for where to get the value for $\widetilde{\text{TJR}}$. As in the method proposed by Li and Wiberg,[7] the permitted total energy temporal jump may be measured relative to the total energy in the system. Another possibility is to prescribe an initial time step from a priori knowledge about the system, compute the resulting TJR and use the TJR from the respective last slab as $\widetilde{\text{TJR}}$.

The adaptive global time-stepping algorithm works as follows: After every time slab, the TJR_n is computed according to Eq. (32). It is checked whether $\text{TJR}_n < \text{TJR}_{\max}$. If not, the time slab is recomputed with a corrected time step; otherwise the time step for the next slab is predicted according to Eq. (33), and the computation proceeds in time.

The method described tries to predict the optimal time step for the next time slab from the data of the actual time step. This procedure works fine if the underlying physics are smooth in time, that is, loading conditions, etc., do not change abruptly. To avoid the rejection of a newly predicted Δt_{N+1} if the solution changes significantly from I_N to I_{N+1}, we prescribe $\text{TJR}_{\max} \approx 1.1, \ldots, 1.5 \cdot \widetilde{\text{TJR}}$.

Compared to the time-stepping method proposed by Li and Wiberg,[7] where Δt is adapted in intervals, the present approach adapts the global time step continuously in every time slab. This is a very natural approach and proved to be both efficient and robust. Furthermore, in the case of sufficiently smooth solutions, no recomputations of complete space–time slabs are necessary.

B. Local Adaptivity in Space and Time

The adaptive method described in Sec. VII.A is useful and easy to implement. Nevertheless, the adaption of the global time step independent of the spatial discretization has several disadvantages.

First, in the case of wave propagation phenomena, both the temporal and the spatial resolution influence the quality of the solution. From the physics point of view, local high gradients in time usually stride along with local high gradients in space. Thus, spatial and temporal adaptivity should be used simultaneously.

Furthermore, the phase and amplitude errors and the filtering characteristics of the finite element discretization vary, dependent on the local Courant number C_i defined in Eq. (31). The errors are usually lowest near $C_i \approx 1$ and may grow significantly for increasing C_i.

Because the correct representation of wave propagation is crucial for elastodynamics, it is useful to limit the Courant number to get the best results.

In the present work, we suggest local space–time adaptive mesh refinement[21] in regions of high TJR to increase the quality of the solution and to decrease the computational effort at the same time.

VIII. Numerical Results

To demonstrate the performance of the space–time finite element method for transient elastodynamics, the elastic wave propagation in Timoshenko beams is investigated. Two different cases are examined (see Fig. 5). Case a deals with a straight elastic beam of length $l = 2$ m without geometric nonlinearities (Fig. 5a), whereas case b treats a geometrically nonlinear circular arch with identical material properties and an initial vertical position of the center $w_0(x = 0) = 0.087485$ m (Fig. 5b). Starting from the undisturbed equilibrium initial condition $\boldsymbol{u}' = \dot{\boldsymbol{u}}' = \boldsymbol{0}$, an impulse load

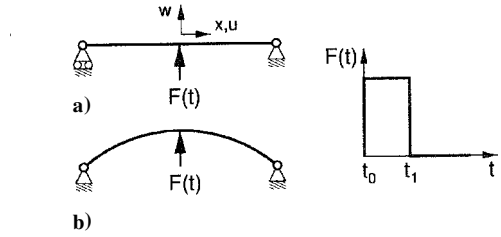

Fig. 5 Test cases for the beam with impulse load: a) linear Timoshenko beam and b) nonlinear, curved Timoshenko beam.

$$F(t) = \begin{cases} \hat{F} = 10^6 N, & 0 < t < 10^{-5}\ \text{s} \\ 0, & \text{otherwise} \end{cases} \tag{34}$$

is applied at the center of the beam at $x = 0$. The impulse load has been chosen because it excites an infinite number of eigenfrequencies and for this reason represents a worst-case scenario for the time domain numerical simulation of wave propagation. Furthermore, there exists an analytic solution for comparison.[22]

The properties of the beam are $E = 5.2 \times 10^{10}$ N/m^2, $A = 0.0012$ m^2, $I = 1.6 \times 10^{-7}$ m^4, $G = 2 \times 10^{10}$ N/m^2, $A_s = 0.001$ m^2, and $\rho = 1000$ kg/m^3. Because of the symmetry of the system, only half of the beam is discretized.

A. Beam with Impulse Load

In Fig. 6, the space–time history of the vertical displacement for the right-half of the beam of case a is given. At the center of the beam at $x = 0$ the symmetry conditions $u = \varphi = 0$ and at $x = 1$ the boundary conditions $u = w = 0$ are applied. The $P1$–$P1$ method with linear interpolations in space is used.

In Fig. 6a, the TDG solution for 100 elements with $\Delta x = 0.01$ m and $\Delta t = 10^{-5}$ s with the resulting Courant numbers $C_1 = 7.3$ and $C_2 = 4.5$ is depicted. Although the TDG scheme filters out some of the high-frequency contributions, the solution is very close to the analytic solution given by Weigand.[22]

The TDG solution for 22 elements in space ($C_1 = 1.7$ and $C_2 = 1.0$) is quite bad (Fig. 6b). The reason for this is the coarse spatial resolution of the wave propagation phenomena, which results in a severe phase error. The disturbance generated by the impulse load at the center of the beam travels outward, is reflected at the support, and travels back toward the center. However, due to the coarse spatial resolution, the waves reach $x = 0$ much too early. Because of the wrong wave speed, the whole solution is deteriorated.

B. Least-Squares Stabilization

Figure 7 shows the time history of the vertical displacement $w(x = 0, t)$ and velocity $\dot{w}(x = 0, t)$ at the center of the beam for test case a. The $P1$–$P1$ method with quadratic interpolations in space is employed. The half beam is discretized with 50 elements and a time step of $\Delta t = 2 \times 10^{-7}$ s is used, which results in a Courant number $C \approx 0.05$.

The applied impulse load Eq. (34) represents a discontinuity in time with an infinite Fourier spectrum. Thus, from the mathematical point of view, an infinitely small time step is necessary to capture all details. Figure 8 shows the slow convergence of the series expansion of the analytical solution by Weigand,[22] where n is the number of series terms considered.

For the present engineering analysis with a finite time step, the discontinuity causes severe oscillations of the velocity $\dot{w}$ in time when the standard TDG scheme is applied (see Fig. 7c). Nevertheless, for the present linear system, these oscillations do not appear in the displacement unknowns $\boldsymbol{u}$ thanks to the filtering characteristics (see Fig. 2) of the weak enforcement of the identity Eq. (10).

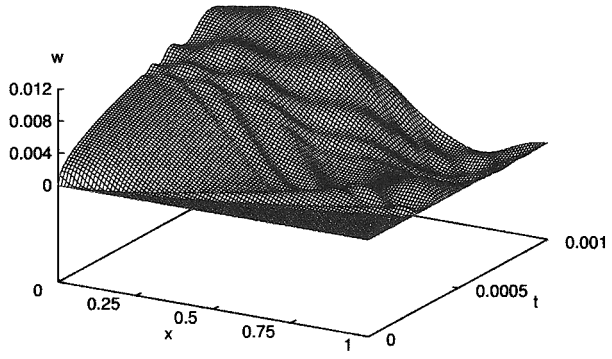

a) TDG, 100 elements

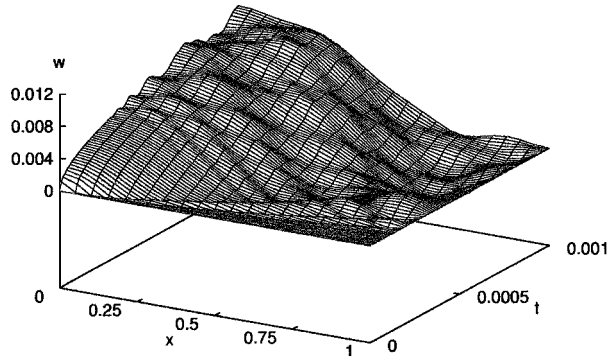

b) TDG, 22 elements

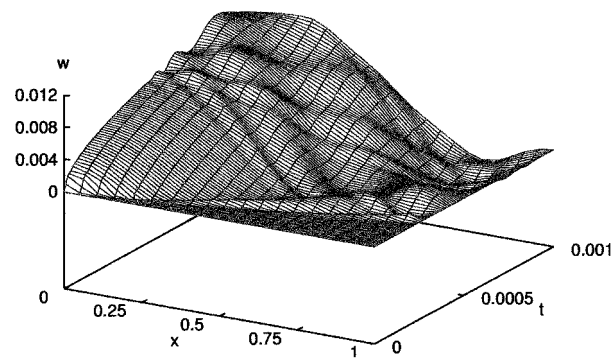

c) G∇ LS$_{\mathcal{F}}$, 22 elements

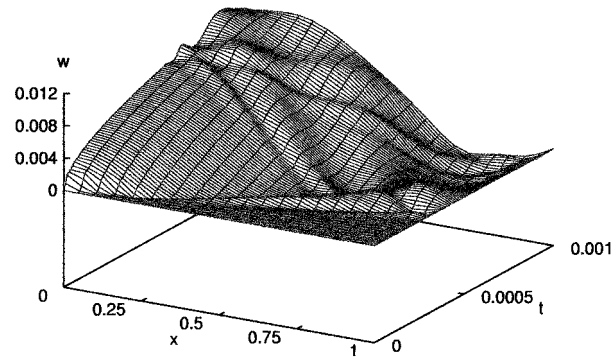

d) G∇ LS$_{\omega \to 0}$, 22 elements

Fig. 6 Beam with impulse load: space–time history of the vertical displacement $w(x, t)$.

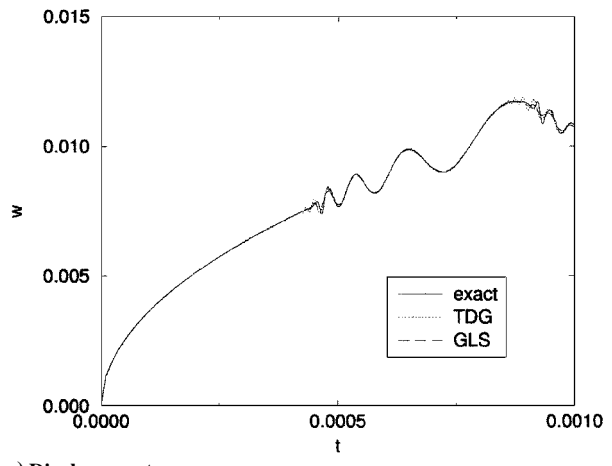

a) Displacement

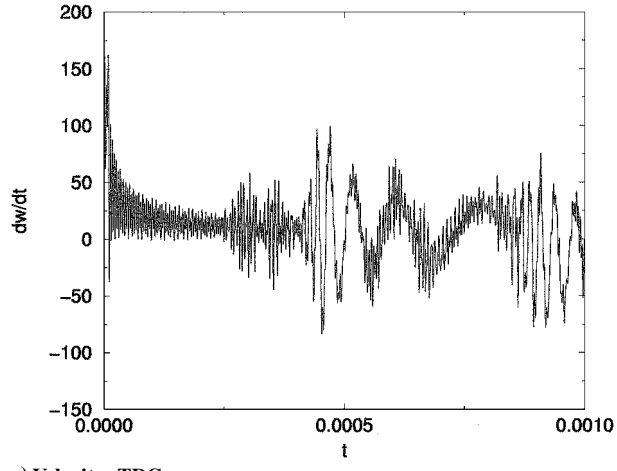

c) Velocity: TDG

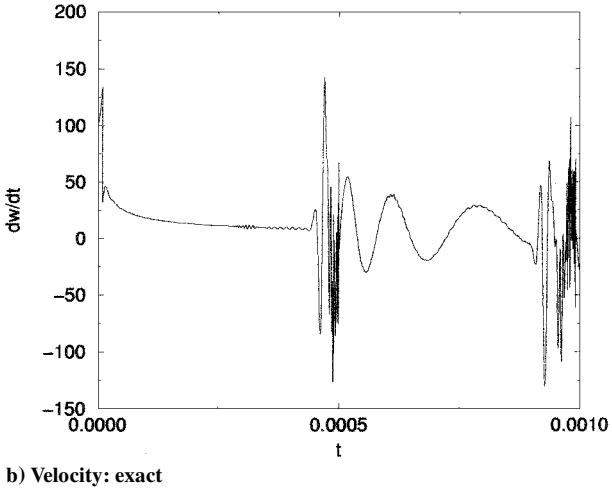

b) Velocity: exact

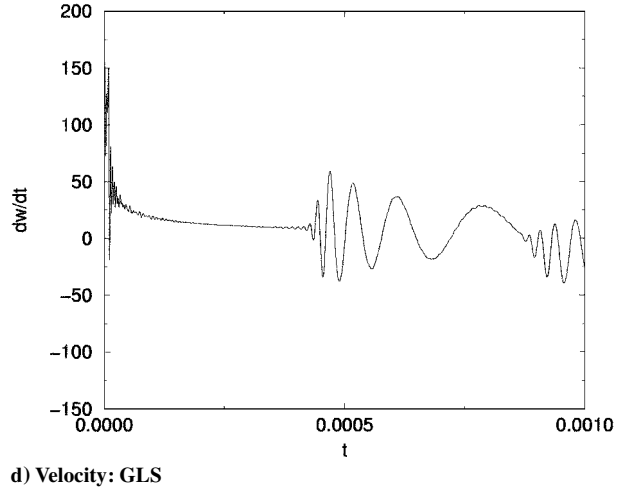

d) Velocity: GLS

Fig. 7 Beam with impulse load: time history of the vertical displacement $w(x = 0, t)$ and velocity $\dot{w}(x = 0, t)$.

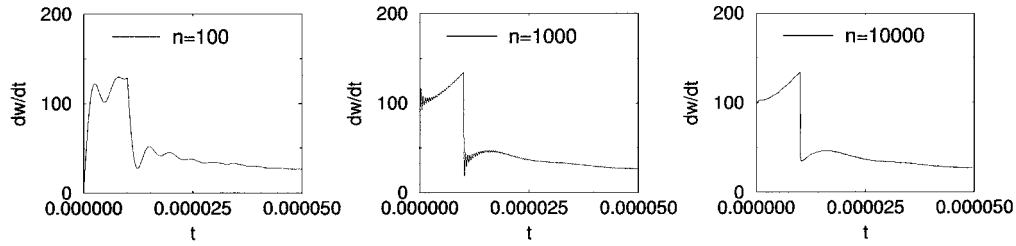

Fig. 8 Beam with impulse load: convergence of the analytical solution series expansion[22] for the velocity $dw/dt(x = 0, t)$.

Additional least-squares stabilization suppresses the spurious, numerical oscillations of the velocity significantly (see Fig. 7d). Unfortunately, some of the very high-frequency contributions of the exact solution are also filtered out. Despite the significant improvement by means of the GLS formulation, an additional nonlinear discontinuity capturing operator is necessary to avoid the remaining oscillations. Because the present test example involves linear physics only, the DC operator is omitted to avoid the additional computational effort that would be necessary to solve iteratively the nonlinearity of the DC operator.

C. Generalized Least-Squares Stabilization

To improve the TDG solution for the coarse spatial discretization of Sec. VIII.A, the Galerkin/generalized least-squares operators described in Sec. V are applied. The results are shown in Fig. 6 on the right-hand side.

The G∇LS$_{\mathcal{F}}$ method gives very good results. The large phase error observed for the TDG method with 22 elements in space is corrected, and the wave speeds are represented well. The solution is nearly identical to the TDG solution employing 100 elements.

In contrast, the G∇LS$_{\omega \to 0}$ method does not perform well. Whereas the large-wavelength contributions seem to be fine, the short-wavelength portion is deteriorated. This can easily be seen at $x = 0$, where the reflected disturbances arrive much too late. This result is not surprising. The design of the method forces the phase error for waves with $\omega \to 0$ to be zero, but it does not give any restrictions on the short-wavelength disturbances. Thus, the long-wavelength propagation is optimized at a cost to the short waves.

The present approach is based on the G∇LS in space, whereas the TDG time-stepping scheme remains basically unchanged. Ultimately, the asymptotic annihilation property of the TDG two-field formulation (Hulbert[16]) discriminates the resolved scales from the subgrid scales. The G∇LS guarantees the optimal numerical representation of the resolved scales, whereas the TDG filters away the unresolved, irrelevant remainder.

Summarizing, the G∇LS approach has successfully been applied for the transient computation of elastic wave propagation in Timoshenko beams employing TDG space–time finite elements. In accordance with the analysis in space by Grosh and Pinsky,[6] the spatial resolution requirements have been reduced significantly without loss of accuracy. Nevertheless, the comparison shows that the optimal design criteria are the critical points. They have to suit the physics of the problem investigated, for example, in the present test case the infinite spectrum of waves excited by the impulse load.

D. Global Adaptive Time Stepping

The global adaptive time stepping described in Sec. VII is applied to test case a. The half beam is discretized with 400 $P1$–$P1$ linear elements. The actual TJR$_n$ is computed in the integral norm, and $\widetilde{\text{TJR}} = 10$ is used.

Figure 9 presents the results. In Fig. 9c the vertical displacement at the center node of the beam is given and shows very good agreement with the exact solution.[22] Figure 9b shows the total time step history, and Fig. 9a, the time step history during the impulse load is shown in detail. Both when the load is applied at $t = 0$ and taken away at $t = 10^{-5}$ s, Δt is automatically refined. Throughout the time domain, Δt varies by about a factor of 100. The Courant numbers are $C_1 \approx 0.8$ and $C_2 \approx 0.5$ at $t \approx 10^{-5}$ s and $C_1 \approx 78$ and $C_2 \approx 48$ toward the end of the computation.

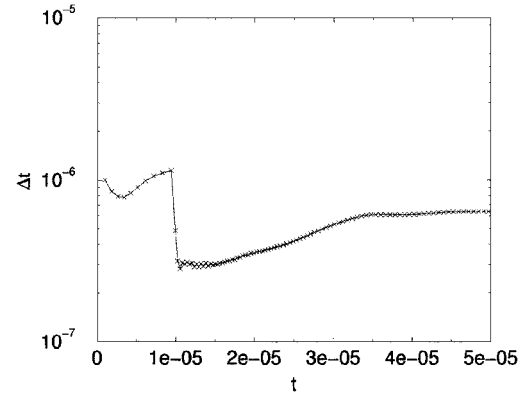

a) Time history of the time step $\Delta t(t)$ (detail)

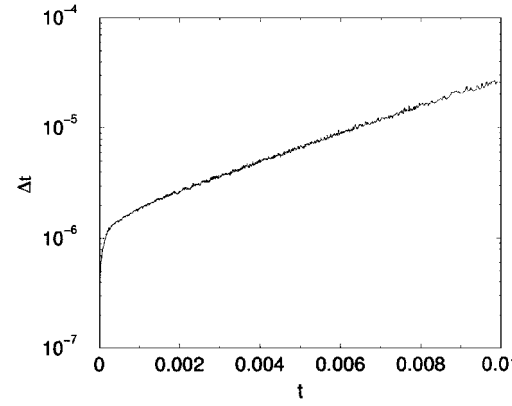

b) Time history of the time step $\Delta t(t)$ (total)

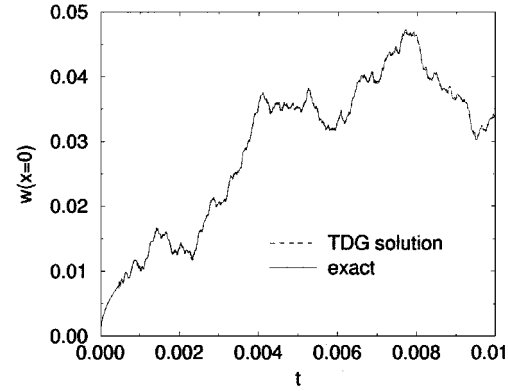

c) Time history of the central vertical displacement $w(x = 0, t)$

Fig. 9 Global adaptive time stepping.

The long-term time step history depicted in Fig. 9b shows small-scale oscillations. Because the adaptive strategy attempts to optimize the time step permanently, the high-frequency oscillating behavior of the beam (Fig. 9c) shows up in $\Delta t(t)$ also.

The present test case demonstrates the contradictory requirements for time stepping. On the one hand, the initial impulse load demands very fine time steps, whereas on the other hand, larger Δt is desirable for the long-term oscillation behavior. In the present computation, the final time step could not even resolve the initial impulse load.

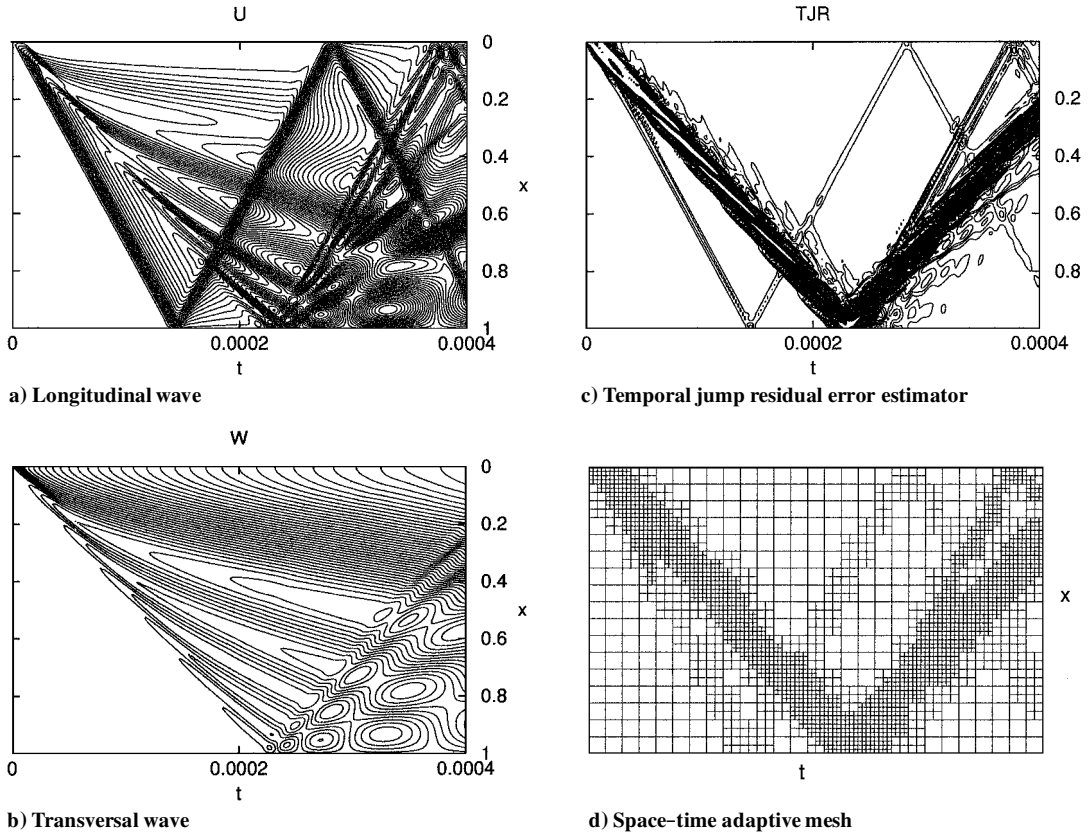

a) Longitudinal wave

c) Temporal jump residual error estimator

b) Transversal wave

d) Space–time adaptive mesh

Fig. 10 Nonlinear wave propagation in space and time.

E. Local Adaptivity

The global time-stepping strategy examined in Sec. VIII.D is robust and efficient. Nevertheless, due to the wide variation of Δt with Δx held constant, the Courant number varies a lot. Thus, the amplitude and phase errors of the underlying finite element discretization may grow undesirably.

In Fig. 10 numerical results for test case b using $P1$–$P1$ TDG elements ($\Delta t = 2 \times 10^{-6}$ s) with linear interpolations in space ($\Delta x = 0.005$ m) are shown. The initial vertical impulse load generates two waves traveling with different wave speeds according to Eq. (6). Because of the geometric nonlinearity of the Timoshenko beam model, a u wave is generated also.

In Fig. 10c the space–time history of the local TJR(x, t) according to Eq. (32) is shown. Both the longitudinal and transversal waves can be identified. Because the u wave is generated indirectly through the nonlinear interactions only, it contains much less energy than the bending wave and causes less error in terms of TJR.

In regions of high TJR, an adaptive mesh refinement simultaneous in space and time keeping the Courant number constant throughout the domain may be done to improve the quality of the solution.

Based on the TJR error indicator, the space–time adaptive mesh shown in Fig. 10d has been generated. The coarsest mesh level consists of 17 elements in space and 27 global time steps. The space–time refinement is carried out to increase the resolution and keep the local Courant number constant throughout the domain without introducing undesirable amplitude or phase errors. Thus, the computational effort can be reduced significantly while maintaining good solution quality.

IX. Conclusions

In the present work, a high-order accurate and efficient method for transient computational elastodynamics has been developed. TDG space–time finite elements with optional GLS and Galerkin/generalized least-squares stabilization are employed.

To suppress spurious numerical oscillations near discontinuities or high gradients, GLS stabilization has been applied. The stabilized formulation filters out underresolved scales of short wavelength without deteriorating the accuracy of well-resolved scales. Particularly, it preserves the order of convergence of the underlying TDG method.

Specially designed G∇LS operators yield excellent improvements of the numerical representation of the elastic wave propagation with respect to phase and amplitude error. Thus, coarser spatial meshes may be used resulting in a significant reduction of computer time. Because of the good results of the spatial G∇LS method for the presented numerical examples involving a large spectrum of frequencies, future research for space–time optimized stabilized methods seems promising. Unfortunately, the complexity of the analysis leading to an optimal design of τ grows significantly in the multidimensional case.

To obtain best possible results with a given number of time steps for both short-term and long-term computations, time adaptivity using the TJR as error indicator has been investigated. The potential benefits of combined space–time adaptivity have been demonstrated for nonlinear elastic wave propagation. In this case, the properties of the finite element discretization with regard to high-frequency damping[16] and local conservation are the driving factors.

Acknowledgment

This research has been financially supported by the Deutsche Forschungsgemeinschaft.

References

[1] Lesiant, P., and Raviart, P., "On a Finite Element Method for Solving the Neutron Transport Equations," *Mathematical Aspects of Finite Elements in Partial Differential Equations*, edited by C. de Boor, Academic Press, New York, 1974, pp. 89–123.

[2] Hughes, T. J. R., and Hulbert, G. M., "Space–Time Finite Element Methods for Elastodynamics: Formulations and Error Estimates," *Computer Methods in Applied Mechanics and Engineering*, Vol. 66, 1988, pp. 339–363.

[3] Johnson, C., "Discontinuous Galerkin Finite Element Methods for Second Order Hyperbolic Problems," *Computer Methods in Applied Mechanics and Engineering*, Vol. 107, 1993, pp. 117–129.

[4] Hulbert, G. M., "Time Finite Element Methods for Structural Dynamics," *International Journal for Numerical Methods in Engineering*, Vol. 33, 1992, pp. 307–331.

[5]Franca, L. P., and Dutra Do Carmo, E. G., "The Galerkin Gradient Least-Squares Method," *Computer Methods in Applied Mechanics and Engineering*, Vol. 74, 1989, pp. 41–54.

[6]Grosh, K., and Pinsky, P. M., "Design of Galerkin Generalized Least-Squares Methods for Timoshenko Beams," *Computer Methods in Applied Mechanics and Engineering*, Vol. 132, 1996, pp. 1–16.

[7]Li, X. D., and Wiberg, N.-E., "Structural Dynamic Analysis by a Time-Discontinuous Galerkin Finite Element Method," *International Journal for Numerical Methods in Engineering*, Vol. 39, 1996, pp. 2131–2152.

[8]Thompson, L. L., and Pinsky, P. M., "A Space-Time Finite Element Method for Structural Acoustics in Infinite Domains; Part 1: Formulation, Stability and Convergence," *Computer Methods in Applied Mechanics and Engineering*, Vol. 132, 1996, pp. 195–227.

[9]Thompson, L. L., "A Multi-Field Space-Time Finite Element Method for Structural Acoustics," *Design Engineering Technical Conferences*, Vol. 3, Pt. B, American Society of Mechanical Engineers, Fairfield, NJ, 1995, pp. 49–64.

[10]Grohmann, B. A., Dornberger, R., Konstanzer, P., and Kröplin, B.-H., "Stabilized Space–Time Finite Elements in Unsteady Aerodynamics and Nonlinear Elastodynamics," *Fourth World Congress on Computational Mechanics*, International Association for Computational Mechanics, Buenos Aires, 1998.

[11]Grohmann, B. A., and Dinkler, D., "Nonlinear Panel Flutter Phenomena in Supersonic and Transonic Flow," *Nonlinear Dynamics* (submitted for publication).

[12]Wallmersperger, T., Grohmann, B. A., and Kröplin, B., "Time-Discontinuous Stabilized Space-Time Finite Elements for PDEs of First- and Second-Order in Time," *European Conference on Computational Mechanics, ECCM '99*, German Association for Computational Mechanics, Munich, 1999, p. 7.

[13]Soulaimani, A., and Fortin, M., "Finite Element Solution of Compressible Viscous Flow Using Conservative Variables," *Computer Methods in Applied Mechanics and Engineering*, Vol. 118, 1994, pp. 319–350.

[14]Shakib, F., "Finite Element Analysis of the Compressible Euler and Navier–Stokes Equations," Ph.D. Dissertation, Dept. of Mechanical Engineering, Stanford Univ., Stanford, CA, Nov. 1988.

[15]Hulbert, G. M., "Discontinuity-Capturing Operators for Elastodynamics," *Computer Methods in Applied Mechanics and Engineering*, Vol. 96, 1992, pp. 409–426.

[16]Hulbert, G. M., "A Unified Set of Single-Step Asymptotic Annihilation Algorithms for Structural Dynamics," *Computer Methods in Applied Mechanics and Engineering*, Vol. 113, 1994, pp. 1–9.

[17]Hughes, T. J. R., *The Finite Element Method—Linear Static and Dynamic Finite Element Analysis*, Prentice–Hall, Upper Saddle River, NJ, 1987, Chap. 9: Exercise 16, pp. 542–550.

[18]Wallmersperger, T., "Stabilisierte Raum-Zeit Finite Elemente für die Strukturdynamik," M.S. Thesis, Inst. für Statik und Dynamik der Luft- und Raumfahrtkonstruktionen, Univ. of Stuttgart, Stuttgart, Germany, July 1997.

[19]Barth, T. J., and Sethian, J. A., "Numerical Schemes for the Hamilton–Jacobi and Level Set Equations on Triangulated Domains," NASA Rept. NAS-97-022, 1997.

[20]Ruge, P., "Hybrid Time-Finite-Elements with Time-Step-Adaption by Discontinuity Control," *Computational Mechanics*, Vol. 17, 1996, pp. 392–397.

[21]Zhou, G., "An Adaptive Streamline Diffusion Finite Element Method for Hyperbolic Systems in Gas Dynamics," TR Preprint 688, Sonderforschungsbereich 123, Univ. of Heidelberg, Heidelberg, Germany, 1992.

[22]Weighand, A., *Einführung in die Berechnung mechanischer Schwingungen, Band III: Schwingungen fester Kontinua (Stäbe und Platten)*, VEB Fachbuchverlag, Leipzig, Germany, 1962.

S. Saigal
Associate Editor